Article | Received 3 January 2024; Accepted 15 April 2024; Published 26 April 2024
https://doi.org/10.55092/rse20240004

Coal-derived porous carbon anodes for Na-ion batteries

Robert Ilango Pushparaj, Xiaodong Hou*, Shuai Xu, Xin Zhang, Bellal Abdelmalek and Ruiqing Zhang

College of Engineering and Mines Research Institute, University of North Dakota, Grand Forks, ND, 58202, USA

* Correspondence author; E-mail: xiaodong.hou@und.edu.

Abstract: Developing low-cost and eco-friendly electrode active materials for sodium-ion battery technologies may increase their competency, allowing them to become the next generation of energy storage systems. Low-cost anode materials are urgently required to address this increasing demand. We propose using earth-abundant coal extracted porous carbon anodes prepared via a facile hydro/solvothermal method followed by carbonization at high temperatures. The surface morphology analysis reveals that the hydrothermal carbon (HTC) and solvothermal carbon (STC) samples are randomly aggregated particles with a hierarchical porous structure. Sodium-ion battery tests indicate that the coal-derived anode exhibits stable cycling and high-rate capabilities. The discharge capacity holds 176 mAh/g and 172 mA/g after the 200th cycle at a current density of 100 mA/g, corresponding to the HTC and STC samples, respectively. Voluble products from coal waste-based anodes exhibit remarkable capacities that reduce anode cost and allow us to produce waste to energy for future secondary battery energy storage.

Keywords: coal; hydrothermal; solvothermal; porous carbon; Na-ion battery

1. Introduction

Na-ion batteries (NIBs) have garnered significant attention as a next-generation power supply for large-scale energy storage due to being created from inexpensive raw materials in the Earth's crust, long cycle life endurance, low-temperature performance, and thermal stability [1–3]. Sodium's physiochemical characteristics are similar to lithium, with a suitable redox potential (−2.71 V SHE) and a lower voltage of approximately 0.3 V. These characteristics indicate that NIBs would be ideal replacements for Li-ion batteries (LIBs) [4,5]. NIBs have significant benefits in terms of lower costs and cyclability; however, a few detriments hinder Na-ion (Na^+) transport, leading to active material volume expansion and impeding commercial applications. The Na^+ ion has a larger ionic size of 1.02 Å vs. Li^+ (0.69 Å), which means it has lower capacity, lower durability, and limited rate capability [6]. Graphite is a

commonly used anode material for LIBs, with a theoretical capacity of approximately 372 mAh/g for LiC_6; however, graphite cannot be used as an anode for NIBs since the Na^+ ion radius does not fit in the small interlayer distance of 0.33 nm [7], which could lead to severe expansion and contraction, eventually worsening electrochemical reaction dynamics.

Many strategies have been established to upgrade NIB electrochemical behavior. Suitable anodes that can be used as an alternative to graphite include hard carbon [8], soft carbon [7], doped graphene [9], and alloys [10]. Hard carbon is currently recognized as the most suitable NIB anode material due to its low average potential and high-rate behavior. Most hard carbon can be fabricated using polymers or biomaterials with reasonable Na^+ storage capacities. For example, Komaba *et al.* [11] reported a hard carbon delivering a reversible capacity of 240 mAh/g at a rate of 25 mA/g; however, they did not discuss its high-rate capabilities, which would have allowed them to understand commercialization perspectives. Researchers have determined that hard carbon can provide reversible capacities of 300 mAh/g [12] and 285 mAh/g [13]; however, this material exhibited an inferior cycling performance. Bai *et al.* [14] recently proposed creating hard carbon derived from PVC nanofibers, achieving 271 mAh/g with a coulombic efficiency of 69.9%, substantially better than the material created from commercial PVC.

Coal-derived carbon, the most affordable energy resource in existence, has recently garnered significant attention [15]. Recent literature indicates that low-rank coal can be extracted and converted to humic acid (HA), then into valuable carbon materials due to the mixture of available organic compounds [16,17]. This carbon can be used as a surface protecting agent, conductive network, and feedstock to synthesize graphene-like materials for various applications [18,19]. Coal-derived carbon and carbon composites have been employed as anode materials for various batteries [20–22]. Recently, Zhao *et al.* [23] prepared carbon anode materials for Na-ion batteries from different grade coal and reported that the defects and oxygen functional groups helps to storage more Na-ions.

We previously used lignite coal-derived graphene to coat SiO anodes for LIBs, which ensured conductivity and improved battery performance [24]; therefore, we believe that highly conductive and low-cost anodes will improve Na-ion diffusion. Controlling the porous and surface area will allow us to improve the overall Na-ion battery's performance. The HTC/STC method effectively prepares the porous and spherical-like carbon anode, which motivates us to synthesize various structured anodes for Na-ion batteries. We used North Dakota coal as a carbon source to prepare porous carbon for use as Na-ion battery anodes. As-prepared anode physical and morphological properties have been investigated using an appropriate analytical tool. We have also examined HTC and STC electrochemical performance and discussed the results in detail.

2. Methods

2.1. Coal-derived porous carbon synthesis

The coal-derived porous carbon was synthesized using a hydrothermal and solvothermal approach, represented schematically in Figure 1. Humic acid (HA) was extracted and purified

from North Dakota lignite using the base extraction procedure from our previous work [25]. A typical hydrothermal route was used to dissolve 3 g of HA in 60 mL of distilled water under constant stirring for three hours to form a homogeneous dissolution. The solution was then transferred into a Teflon-lined autoclave and heated to 200 ℃ for 14 h. The resultant products were naturally cooled to room temperature, then centrifuged and washed several times with distilled water and ethanol before drying at 70 ℃ overnight. The collected black powders were calcined at 1000 ℃ for six hours under an Argon atmosphere at a ramp rate of 5 ℃/min. The same procedure was followed to obtain solvothermal derived carbon, except for using ETOH as a solvent to replace the distilled water. The final samples were collected and labeled as HTC and STC for further analysis.

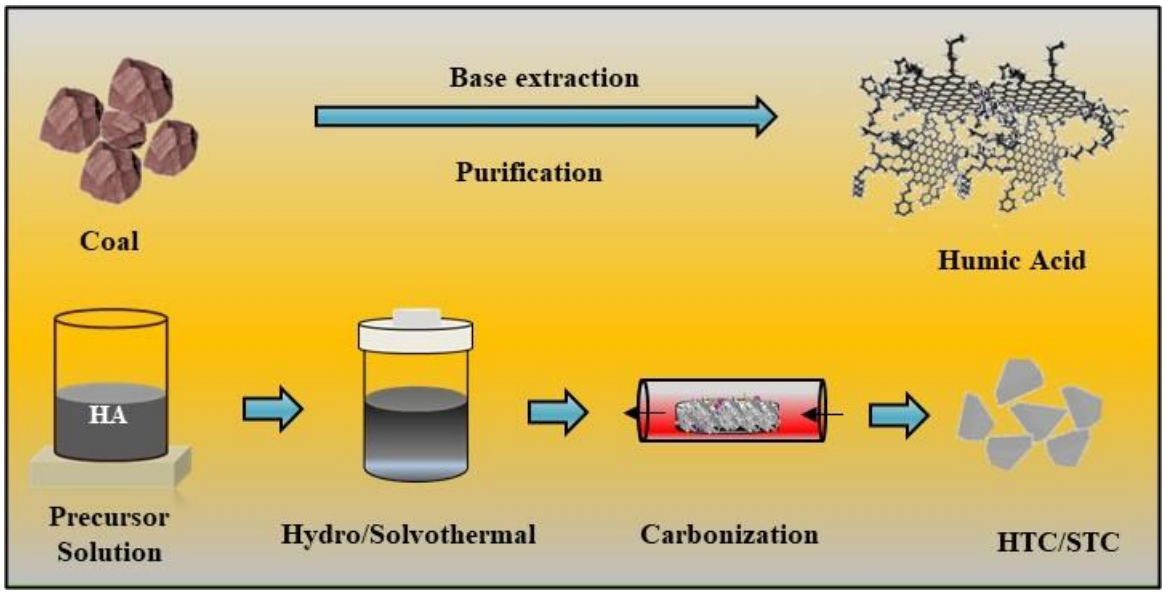

Figure 1. Schematic illustration for the preparation of HTC and STC anode materials.

2.2. Characterization

An X-ray diffractometer (Smartlab, Rigaku) was used to identify the crystal structure operating with a driving voltage of 40 kV and a tube current of 44 mA using Cu Kα radiation, collecting the signal at a scan rate of 3 °/min between 5 ° and 80 °. Brunauer-Emmett-Teller (BET) HTC and STC powder measurements were acquired in a liquid nitrogen atmosphere using an ASAP 2010 analyzer (Micromeritics, USA). Field Emission Scanning Electron Microscopy (FEI Quanta 650 FE-SEM) was used to capture the HTC and STC samples' surface morphologies at different locations.

2.3. Electrochemical measurements

Na-ion battery testing was conducted using a CR-2032 model coin cell in an Ar-filled glove box. The testing electrode was created by mixing an active material (80%), polyvinylidene fluoride (10%), and carbon black (10%) in N-methyl-2-pyrrolidinone (NMP) as a solvent. The suspension was coated on a pretreated Cu-foil, dried in a vacuum oven at 80 ℃ for 12 h,

then cut into a disc shape. The cells were assembled with an HTC/STC anode, metallic 'Na' as the counter electrode, glass fiber (Whatman GF/F) as a separator, and 1M $NaPF_6$ salt in EC:DMC Ethylene carbonate/Dimethyl carbonate (1:1 vol%). As-fabricated cells were examined at different current rates on a galvanostatic cycler at a voltage of 0.01 V–2.0 V (vs. Na^+/Na) using a Neware Battery Testing System (CT-4008, Neware Technology Limited, Shenzhen. China). Cyclic voltammetry (CV) and Electrochemical impedance spectroscopy (EIS) were acquired with a Gamry Series G 750 electrochemical workstation (Gamry Instruments, Warminster, USA). CV profiles were secured with a voltage range of 0.01 V–2.0 V at 0.5 mV s^{-1}. EIS analysis was completed with an AC voltage amplitude of 10 mV and a frequency of 1,000,000 Hz to 0.01 Hz.

3. Results and discussion

The XRD diffraction patterns of the HTC and STC samples are illustrated in Figure 2a. Broad peaks were observed at 2 theta 25 ° and 43 ° from both HTC and STC samples after carbonization. A sharp peak observed on HTC around 40–50 is a characteristic peak from the aluminum sample holder, while this peak not showing on STC is probably due to a larger amount of sample used for the XRD testing. This pattern is similar to low graphitic carbon and can be comparable to our previous studies [24]. In general, low graphitic carbon refers to a material or substance that contains a low proportion of crystalline (ordered) carbon atoms and high proportion of disordered carbon atoms. This can be quantified by using Raman spectroscopy to measure the ratio of D (disordered) and G (graphene) (I_D/I_G). The Raman spectra in Figure 3c shows the nature of the low graphitic carbon of HTC materials, as indicated by the high intensity of D-band. Interestingly, the increase of G-band intensity after carbonization probably implied that more defects or pores are generated during the carbonization process.

We estimated the surface area and pore size, finding that the typical N_2 adsorption-desorption profile exhibited a usual type-IV isotherm and H_2 hysteresis loop with a BJH pore distribution that endorses the mesoporous texture depicted in Figure 2b. The microporous BET method was applied at a very low range of relative pressures between 3.12×10^{-3} and 9×10^{-3}. The increase in N_2 adsorption amount was persistent and strong at high P/P_0 values, indicating the existence of a large open macropore surface that contributes to physical adsorption. The calculated specific HTC surface areas were 49.301 m^2 g^{-1}, and the pore size was 2.518e+01 Å.

The surface morphology examination was identified using FE-SEM analysis. Figure 3a–3d depicts the surface morphology of the HTC and STC samples. The HTC particle shapes were not uniform, and the sizes varied for each particle at a micrometer scale. The HTC and STC samples had many pores on the surface, illustrated in magnified view. These pores may enhance Na-ion diffusion. HTC has obvious pores on the surface compared to STC, as discussed in the previously mentioned BET analysis, While STC samples have smaller particle sizes and wider particle size distribution, which contribute to a large specific surface area and defect sites. These results can explain the lower ICE of STC than HTC in the latter section.

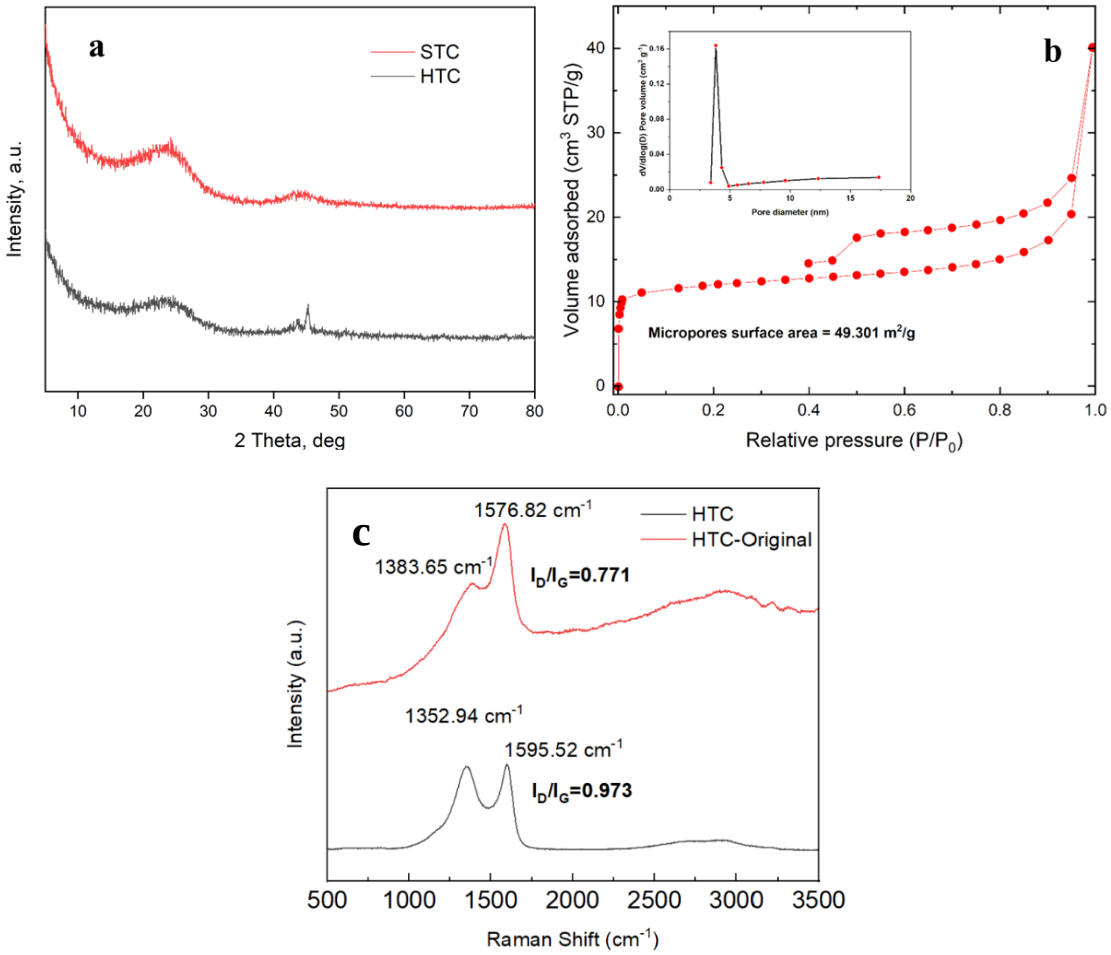

Figure 2. (**a**) XRD pattern for HTC and STC; (**b**) adsorption/desorption isotherm of the HTC sample and pore volume distribution calculated using the BJH method; (**c**) Raman Spectra of HTC samples before and after carbonization.

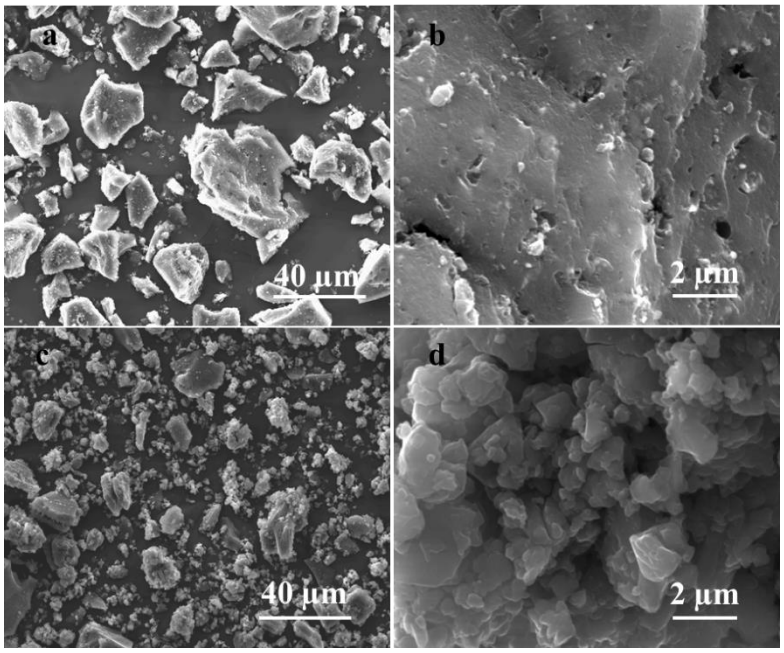

Figure 3. FE-SEM images of (**a,b**) HTC and (**c,d**) STC at different magnifications.

The HTC and STC Na-ion storage mechanisms are explained by the CV profiles provided in Figure 4a–4b. The CV profiles were collected between the voltage range of 0.01 V–2 V for the first five cycles at a scan rate of 0.5 mV/s. This profile was composed of reduction and oxidation peaks between the given voltage window. A small reduction peak at about 0.4 V and a weak hump at about 0.7 V were observed in the first cycle of the CV profiles for both HTC and STC samples. These peaks are widely accepted to originate from electrolyte decomposition and side-reactions between electrolyte and hard carbon anode, leading to the formation of a solid electrolyte interface (SEI). The disappearance of these peaks in the following cycles supports our hypothesis, as the side reactions and SEI formation predominantly occurred in the first cycle [26]. A weak peak, exhibited at 0.1 V, originated from the cathodic and anodic peaks created by Na-ion insertion and extraction into the hard carbon anodes [27]. Furthur subsequent cycles were virtually overlapped, ensuring the high reversibility of Na-ions during Na intercalation and de-intercalation.

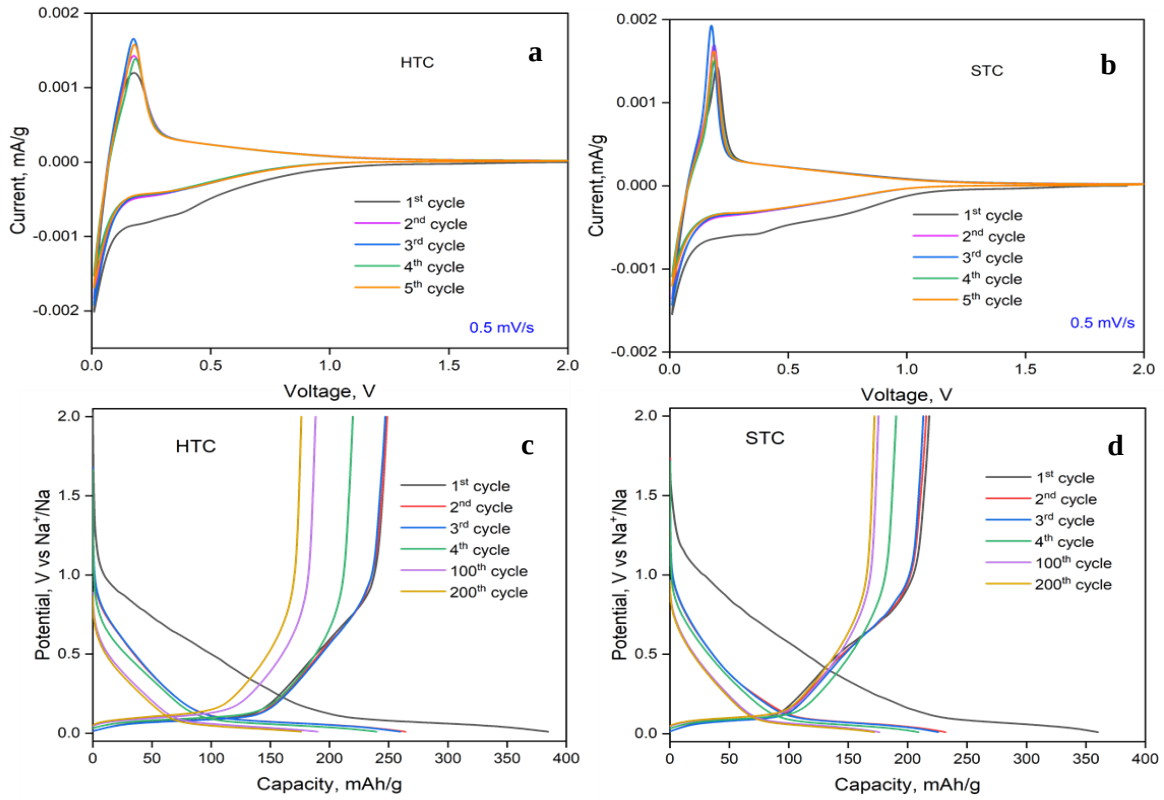

Figure 4. (**a,b**) Cyclic voltammetry curves at 0.5mV/s, and (**c, d**) discharge and charge profiles of the HTC and STC samples.

The discharge and charge profiles of the HTC and STC samples cycled at a current density of 10 mA/g for the first few cycles, followed by a current of 100 mA/g over 200 cycles. The potential slope was well-matched with the CV profile, indicating the Na-ion intercalation occurred at around 0.1 V. The discharge and charge capacities were 385/249 mAh/g, 264/249 mAh/g, 260/247 mAh/g, 240/220 mAh/g, 190/188 mAh/g, and 176/176 mAh/g for the 1st, 2nd, 3rd, 4th, 100th, and 200th cycles, respectively, corresponding to the HTC samples

(Figure 4c). The ICE was approximately 65%, and the ICE increased and maintained at 98–100% after a few cycles. The STC samples delivered discharge and charge capacities of 360/218 mAh/g, 232/216 mAh/g, 226/213 mAh/g, 209/190 mAh/g, 176/176 mAh/g, and 172/172 mAh/g for the 1st, 2nd, 3rd, 4th, 100th, and 200th cycles, respectively Figure 4d. The STC samples had a lower ICE of 61% than the HTC samples; however, they increased and maintained at 99–100% over 200 cycles, proving the material's stability. The typical ICE loss due to the SEI and possible side reactions was caused by the functional groups and irreversible Na-ions [28].

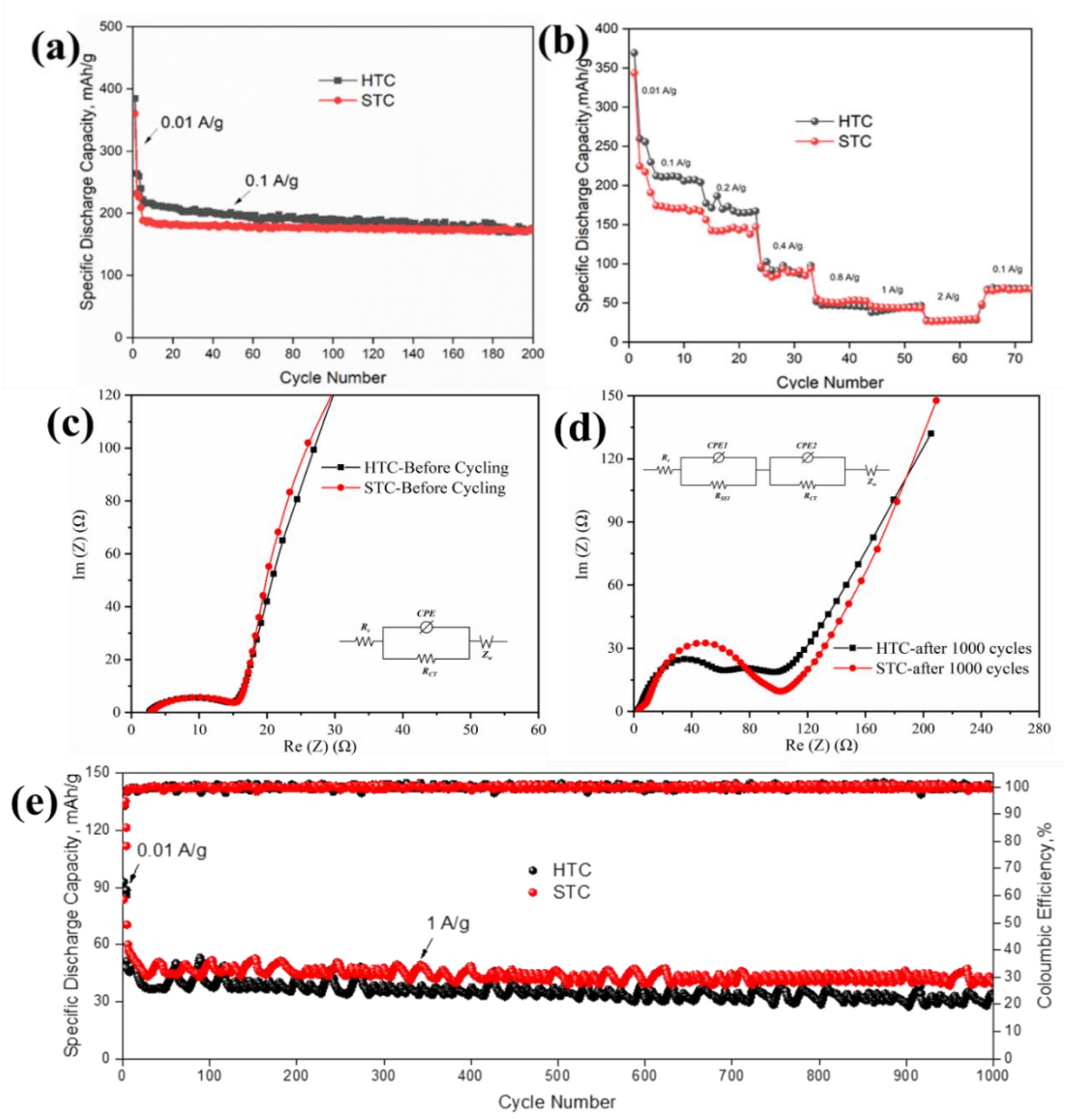

Figure 5. (**a**) Cycling performance; (**b**) rate capability; (**c**) electrochemical impedance spectroscopy of HTC and STC before cycling and corresponding equivalent circuit; (**d**) electrochemical impedance spectroscopy of HTC and STC after cycles and the corresponding equivalent circuit, and (**e**) long-term cycling performance of the HTC and STC samples.

Figure 5a depicts the HTC and STC samples' cycling performance. The cells were cycled at a low current density of 10 mA/g for the first three cycles, then at 100 mA/g. The HTC sample retained approximately 176 mAh/g after 200 cycles with a coulombic efficiency (CE) of 100%, whereas the STC samples maintained approximately 172 mAh/g with a CE of 100%. Both anodes maintained stable cycling performance after 200 cycles, indicating the stability of as-prepared anodes from coal. The cells were tested with different current densities at ten cycle intervals to illustrate the stability tests further. Figure 5b shows the rate capacity tests for the HTC and STC samples at different current densities of 10 mA/g, 100 mA/g, 200 mA/g, 400 mA/g, 800 mA/g, 1000 mA/g, and 2000 mA/g. The results indicate that the discharge capacity was higher for the HTC samples than the STC samples at a low current rate, while the discharge capacity was approximately the same when the current density was increased by 10 or 20x. The capacities of the HTC and STC samples recovered to 66 mAh/g when the cell cycled back to 100 mA/g, corresponding to the anodes' remarkable rate capability.

The electrochemical impedance principle of the HTC and STC samples was examined using Nyquist plots (Figure 5c–5d), which are composed of semicircles in high-frequency zones and straight slopes at low-frequency zones, corresponding to charge transfer resistance (Rct) and Warburg impedance (Z_w). The calculated R_{ct} values were 14 Ω 16 Ω for HTC and STC, respectively, before cycling. After charging/discharging for 1000 cycles, both EIS spectra exhibited two semicircles located at high and medium frequency regions over 1000 cycles. The first semicircle belongs to Na-ion diffusion through the solid electrolyte interface, and the next semicircle was attributed to R_{ct} (38.4 Ω for HTC and 88.3 Ω for STC) at the electrode and electrolyte interface. These findings reveal that the resistance of the HTC samples was slightly diminished after long-term cycling due to their porous nature, which allows Na-ion diffusion. As-prepared HTC and STC electrodes were assessed at a high current density of 1 A/g to examine their long-term cycling stability (Figure 5e). Both electrodes became stable after the first three cycles and maintained 150 mAh/g and 150 mA/g after 1000 cycles, which is ascribed to HTC and STC. These results suggest that stable SEI formed on the surface after pre-lithiation, which aids in diffusing the Na-ion without any barrier. We captured the surface morphology of the cycled electrode after 1000 cycles to better understand the cycled electrode surface.

Figure 6 depicts the HTC and STC images after 1000 cycles of charging and discharging. Surface films (SEI) were observed on the HTC (Figure 6a–6b) and STC (Figure 6c–6d) electrodes' surfaces at low and high magnifications. Significant surface changes occurred after 1000 cycles compared to before cycling due to electrolyte decomposition and SEI formation. After 1000 cycles, the surface morphology of HTC and STC samples are showing a thin, uniform SEI formed on the surface, which is beneficial for allowing stable Na-ion insertion and extraction during the discharge and charge process. The continuous and uniform formation of SEI may act as stable interfacial network, enhancing ion transfer and improving ionic conductivity. Conversely, before cycling, both HTC and STC show well-defined boundaries of each particle. The changes in surface morphology of the electrode particles before and after cycling can serve as a significant indicator of SEI quality. This assertion is demonstrated in our previous research [29], wherein we pioneered a SEM staining technique

for observing SEI formation. It can be noted that the minor pores are not visible due to the formation of SEI later after prolonged cycling. This pore structure provides a large amount of free space between the carbon structure and the appearance of porous structures with micro/nanocavities and/or micro/nanoholes, which are favorable for Na-ion transport.

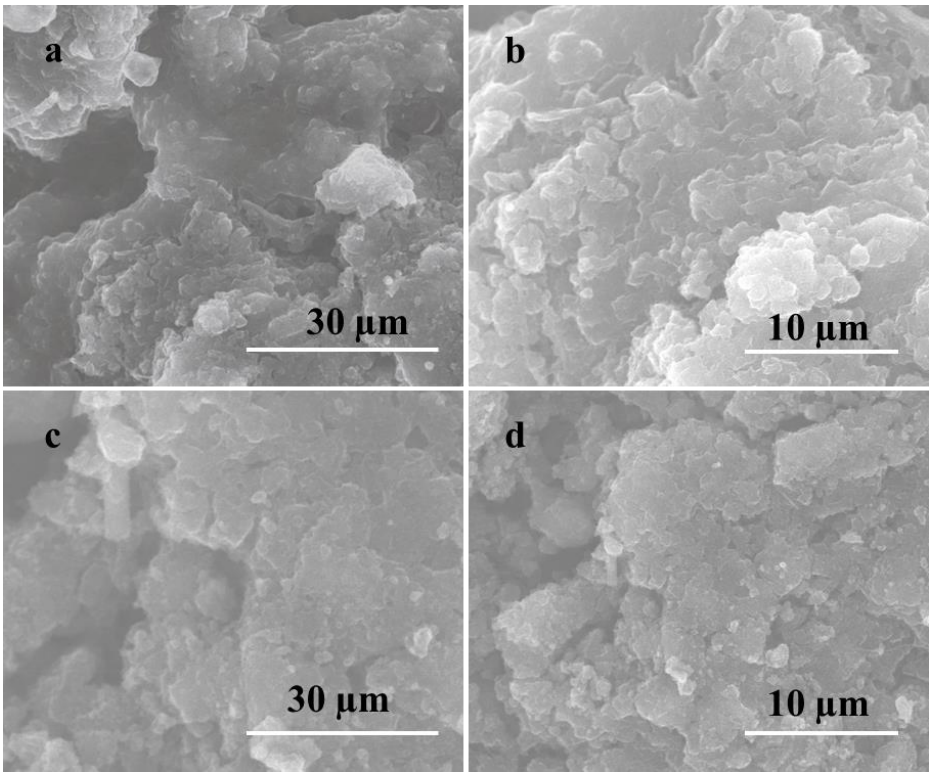

Figure 6. FE-SEM images of (**a,b**) HTC and (**c,d**) STC at different magnifications after long term cycling.

4. Conclusion

We successfully prepared coal-derived porous carbon anode materials via facile hydrothermal and solvothermal methods. As-prepared HTC and STC carbon has been studied for use as an anode electrode for Na-ion battery applications. Their unique porous structure increases reaction kinetics and shortens the Na-ion diffusion pathways, resulting in better cycling and rate capability. HTC and STC exhibit long-term cycling endurance over 1000 cycles at 1 A/g, indicating the material's durability, which was an exciting discovery. The overall comparative analysis demonstrates that low-cost and coal-derived carbon samples can be an alternative anode for replacing the commercial anodes in future generation Na-ion batteries.

Acknowledgments

This work was funded by U.S. Department of Energy with grant number DE-FE-0031984 and the Office of the Vice President for Research at the University of North Dakota with grant number Postdoc Fund FY19.

Conflict of interest

There is no conflict of interest to declare.

Authors' contribution

Conceptualization, X.H.; methodology, R.I.P. and X.H.; formal analysis, R.I.P., X.H, S.X. and B.A.; investigation, R.I.P., X.Z. and R.Z.; resources, X.H.; data curation, R.I.P., S.X., X.Z. and R.Z.; writing—original draft preparation, R.I.P.; writing—review and editing, X.H.; visualization, R.I.P.; supervision, X.H.; project administration, X.H.; funding acquisition, X.H. All authors have read and agreed to the published version of the manuscript.

References

[1] Hwang JY, Myung ST, Sun YK. Sodium-ion batteries: present and future. *Chem. Soc. Rev*. 2017, 46(12):3529–3614.
[2] Vaalma C, Buchholz D, Weil M, Passerini S. A cost and resource analysis of sodium-ion batteries. *Nat. Rev. Mater*. 2018, 3(4):1–11.
[3] Mukai K, Inoue T, Kato Y, Shirai S. Superior low-temperature power and cycle performances of Na-ion battery over Li-ion battery. *ACS Omega* 2017, 2(3):864–872.
[4] Nayak PK, Yang L, Brehm W, Adelhelm P. From lithium‐ion to sodium‐ion batteries: advantages, challenges, and surprises. *Angew. Chemie Int. Edit.* 2018, 57(1):102–120.
[5] Yabuuchi N, Kubota K, Dahbi M, Komaba S. Research development on sodium-ion batteries. *Chem. Rev.* 2014, 114(23):11636–11682.
[6] Li L, Peng S, Bucher N, Chen HY, Shen N, *et al.* Large-scale synthesis of highly uniform $Fe_{1-x}S$ nanostructures as a high-rate anode for sodium ion batteries. *Nano Energy* 2017, 37:81–89.
[7] Cao B, Liu H, Xu B, Lei Y, Chen X, *et al*. Mesoporous soft carbon as an anode material for sodium ion batteries with superior rate and cycling performance. *J. Mater. Chem. A.* 2016, 4(17):6472–6478.
[8] Li Z, Chen Y, Jian Z, Jiang H, Razink JJ, *et al.* Defective hard carbon anode for Na-ion batteries. *Chem. Mater*. 2018, 30(14): 4536–4542.
[9] Zhang F, Alhajji E, Lei Y, Kurra N, Alshareef HN. Highly doped 3D graphene Na‐ion battery anode by laser scribing polyimide films in nitrogen ambient. *Adv. Energy Mater.* 2018, 8(23):1800353.
[10] Yang G, Ilango PR, Wang S, Nasir MS, Li L, *et al.* Carbon-based alloy-type composite anode materials toward sodium-ion batteries. *Small* 2019, 15(22):1900628.
[11] Komaba S, Murata W, Ishikawa T, Yabuuchi N, Ozeki T, *et al*. Electrochemical Na insertion and solid electrolyte interphase for hard‐carbon electrodes and application to Na‐Ion batteries. *Adv. Funct. Mater.* 2011, 21(20):3859–3867.
[12] Stevens DA, Dahn JR. High capacity anode materials for rechargeable sodium‐ion batteries. *J. Electrochem. Soc.* 2000, 147(4):1271.
[13] Alcántara R, Lavela P, Ortiz GF, Tirado JL. Carbon microspheres obtained from resorcinol-formaldehyde as high-capacity electrodes for sodium-ion batteries. *Electrochem. Solid. St.* 2005, 8(4):A222.
[14] Bai Y, Wang Z, Wu C, Xu R,Wu F, *et al.* Hard carbon originated from polyvinyl chloride nanofibers as high-performance anode material for Na-ion battery. *ACS Appl. Mater. Inter.* 2015, 7(9):5598–5604.
[15] Hassan M, Gomes VG. Coal derived carbon nanomaterials – Recent advances in synthesis and applications. *Appl. Mater. Today.* 2018, 12:342–358.

[16] Stevenson FJ. *Humus chemistry: genesis, composition, reactions*. New York: John Wiley & Sons, 1994.
[17] Ikeya K, Sleighter RL, Hatcher PG, Watanabe A. Characterization of the chemical composition of soil humic acids using Fourier transform ion cyclotron resonance mass spectrometry. *Geochim. Cosmochim. Ac*. 2015, 153:169–182.
[18] Powell C, Beall GW. Graphene oxide and graphene from low grade coal: Synthesis, characterization and applications. *Curr. Opin. Colloid. In.* 2015, 20(5–6):362–366.
[19] El-shazly MD, Henderson B, Beall GW. Reduced humic acid nanosheets and its uses as nanofiller. *J. Phys. Chem. Solids.* 2015, 85:86–90.
[20] Duraia ESM, Niu S, Beall GW, Rhodes CP. Humic acid-derived graphene–SnO_2 nanocomposites for high capacity lithium-ion battery anodes. *J Mater Sci: Mater. Electron.* 2018, 29(10):8456–8464.
[21] Abou-Rjeily J, Laziz NA, Autret-Lambert C, Sougrati MT, Toufaily J, *et al.* Bituminous coal as low‐cost anode materials for sodium‐ion and lithium‐ion batteries. *Energy Technol-ger*. 2019, 7(7):1900005.
[22] Xiao N, Zhang X, Liu C, Wang Y, Li H, *et al.* Coal-based carbon anodes for high-performance potassium-ion batteries. *Carbon* 2019, 147:574–581.
[23] Zhao H, Zhao D, Ye J, Wang P, Chai M, *et al.* Directional oxygen functionalization by defect in different metamorphic‐grade coal‐derived carbon materials for sodium storage. *Energy Env. Mater.* 2022, 5(1):313–320.
[24] Xu S, Zhou J, Wang J, Pathiranage S, Oncel N, *et al* , In situ synthesis of graphene-coated silicon monoxide anodes from coal‐derived humic acid for high-performance lithium-ion batteries. *Adv. Funct. Mater.* 2021, 31(32):2101645.
[25] Pushparaj RI, Cakir D, Zhang X, Xu S, Mann M, *et al.* Coal-derived graphene/MoS_2 heterostructure electrodes for Li-ion batteries: experiment and simulation study. *ACS Appl. Mater. Inter.* 2021, 13(50):59950–59961.
[26] Sun N, Liu H, Xu B. Facile synthesis of high performance hard carbon anode materials for sodium ion batteries. *J. Mater. Chem. A*. 2015, 3(41):20560–20566.
[27] Zhu X, Jiang X, Liu X, Xiao L, Cao Y. A green route to synthesize low-cost and high-performance hard carbon as promising sodium-ion battery anodes from sorghum stalk waste. *Green Energy Environ*. 2017, 2(3):310–315.
[28] Kan J, Wang H, Zhang H, Shi J, Liu W, *et al.* Nitrogen functionalized carbon nanocages optimized as high-performance anodes for sodium ion storage. *Electrochim. Acta*. 2019, 304:192–201.
[29] Zhang X, Hou X, Hou Y, Zhang R, Xu S, *et al.* Insights into chemical prelithiation of SiO_x/Graphite composite anodes through scanning electron microscope imaging. *ACS Appl. Energy. Mater.* 2023, 6(15):7996–8005.